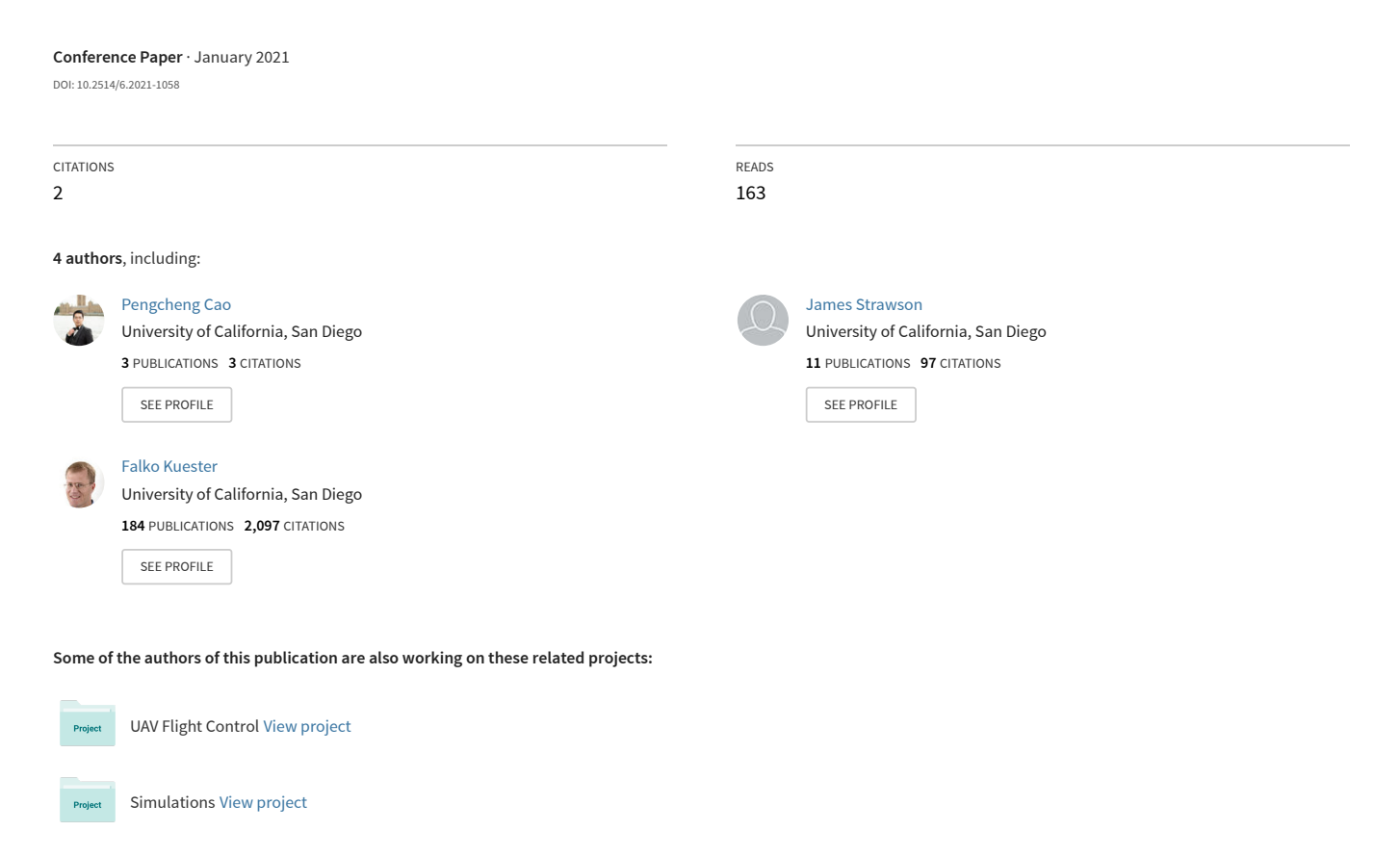
# Decoupled Translational and Rotational Flight Control Designs of Canted-Rotor Hexacopters



# Decoupled Translational and Rotational Flight Control Designs of Canted-Rotor Hexacopters

Pengcheng Cao\*, James R. Strawson<sup>†</sup>, Thomas R. Bewley <sup>‡</sup>, and Falko Kuester <sup>§</sup> *University of California San Diego, La Jolla, CA 92093, USA* 

The mainstream designs of the multi-rotor UAVs typically arrange their motors and propellers near or in the same plane, imposing limitations on their control maneuvers due to under-actuation. The limited control maneuvers cause the multi-rotors to have to pitch and roll in order to perform lateral translations. These multi-rotor aerial vehicles also lose the capability of keeping their center-of-mass stationary in the air while rotating by a certain pitch or roll angle due to the thrusts generated along rotated vertical axis in the body frame. This paper presents the mathematical model of a hexacopter with rotor-axes tilted to enhance the control maneuverability of conventional multi-rotor UAVs. Based on the Newton-Euler formalism of dynamics, we propose the path tracking controller and the tilt-hovering controller for canted-rotor hexacopters. First, the path tracking controller decouples lateral movements from pitch and roll rotations of the vehicle. Second, the tilt-hovering controller stabilizes the position of the center of mass of the vehicle as well as its orientation while it is rotated by a certain pitch or roll angle. Numerical simulations are performed to corroborate the mathematical model and control designs, and to compare with the performance of conventional multi-rotor UAVs.

#### I. Nomenclature

```
\mathcal{F}_{E}
                Earth-fixed inertial frame
                hexacopter body frame
\mathcal{F}_{m_i}
                local frame of i-th rotor (motor-propeller group)
O_B
                hexacopter center of mass (CoM) and origin of \mathcal{F}_B
O_E
                origin of \mathcal{F}_E, coincident with O_B before hexacopter takes off
                center of each rotor and origin of \mathcal{F}_{m_i}
O_{m_i}
\mathbf{R}_{EB}
                rotation matrix from \mathcal{F}_B to \mathcal{F}_E
\mathbf{T}_{EB}
                body rotation angles transformation matrix from \mathcal{F}_B to \mathcal{F}_E
                rotation matrix from \mathcal{F}_{m_i} to \mathcal{F}_B, where i = 1 \dots 6
\mathbf{R}_{Bm_i}
          =
          =
                the positions of O_{m_i} in body frame \mathcal{F}_B, where i = 1 \dots 6
\mathbf{p}_{Bm_i}
                rotor-axis rotation angle around X-axis of \mathcal{F}_{m_i}, where i = 1 \dots 6
                rotor-axis rotation angle around Y-axis of \mathcal{F}_{m_i}, where i = 1 \dots 6
\theta_i
                the i-th rotor arm's yaw angle with respect to the body X-axis, where i = 1 \dots 6
                unit vector indicating orientation of i-th rotor-axis, where i = 1 \dots 6, V_i \in \mathbb{R}^3
V_i
Φ
                3-tuple of (\phi_1, \phi_2, \phi_3)
Θ
          =
                3-tuple of (\theta_1, \theta_2, \theta_3)
                the intermediate force vector consisting of the square of each rotor's rotary speed, \Omega \in \mathbb{R}^6
Ω
                [x_E, y_E, z_E]^T, the linear displacement/position vector in \mathcal{F}_E
ξ
                the moments of inertia matrix in \mathcal{F}_B, \mathbf{I}_B \in \mathbb{R}^{3\times 3}
\mathbf{I}_{B}
                the vehicle's angular velocity in \mathcal{F}_B, \eta_B \in \mathbb{R}^3
\eta_B
                the vehicle's angular velocity in \mathcal{F}_E, \eta_E \in \mathbb{R}^3
\eta_E
```

<sup>\*</sup>Ph.D. student, Department of Mechanical and Aerospace Engineering, University of California, San Diego, 9500 Gilman Dr, La Jolla, CA 92093: p5cao@eng.ucsd.edu.

<sup>†</sup>Robotics Engineer, ModalAI, Inc., 10855 Sorrento Valley Rd Ste. 2, San Diego, CA 92121; jstrawso@gmail.com

<sup>&</sup>lt;sup>‡</sup>Professor, Department of Mechanical and Aerospace Engineering, University of California, San Diego, 9500 Gilman Dr, La Jolla, CA 92093; bewley@eng.ucsd.edu.

<sup>§</sup>Professor, Department of Structural Engineering, University of California, San Diego, 9500 Gilman Dr, La Jolla, CA 92093; fkuester@eng.ucsd.edu.

 $K_{\xi}$  = the gain matrix for translational control  $K_R$  = the gain matrix for rotational control

#### **II. Introduction**

Multi-rotors are currently one of the most prevalent types of Unmanned Aerial Vehicle (UAV) platforms applied to various research, commercial, industrial, or hobbyist purposes. They are frequently deployed and utilized for applications in areas including aerial imaging [1] and manipulation [2]. Among all multi-rotors, although the vehicles with the configuration of 4 rotors, namely quadcopters, are advantageous due to its simplicity of design and manufacturing, the 6-rotor configuration drones, namely hexacopters, perform better in reliability due to the tolerance to the failure of one or two motors [3], and generally with greater agility due to more thrust provided by 2 extra motors. Moreover, the standard quadcopters have to rely on rolling and pitching to generate lateral forces, result in an under-actuated system which cannot track an arbitrary flight path in its 6 degrees of freedom (DoF). Although some researchers have proposed canted-rotor quadcopter designs [4][5], their involvement of extra actuators for extra DoFs can increase the battery consumption and control latency and complexity.

While hexacopters, on the other hand, can be rendered as a fully-actuated system if it is configured with canted rotor-axes[6]. A standard hexacopter design align all its six propellers in parallel axes, thus maximizing the vertical thrust force and improving its redundancy and capability of carrying payload. However, this configuration can only produce an input force parallel to the vertical axis in its body frame. In order to exert lateral forces on the vehicle, the spinning speed of each propeller is controlled to generate roll and pitch torques to rotate the vehicle around Xand Y-axis in the body frame, respectively. The re-oriented vehicle body obtains lateral force components in the XY-plane of the inertial frame as discussed in [7]. The standard multi-rotor configurations result in the vehicle dynamics coupling the pitch and role angles with both lateral and vertical force components in the inertial frame. In this case, the hexacopter's pitch and roll angles cannot be controlled at will without affecting its translational motions, such that the lateral translations of the hexacopter are not directly controlled. In order to decouple hexacopter's lateral translations from pitching and rolling, some of the canted-rotor hexacopters are installed with extra actuators to realize fully actuated maneuvers[8], while others obtain full 6-DoF control authorities via specific rotor layout targeting omni-directional flight[9], or via deviating the rotor axes from the vertical axes by optimized canted and dihedral angles[10]. Moreover, although the coupled multicopter dynamics is proven to be deferentially flat thus making it capable of tracking smooth trajectories [11], the hexacopter configuration with the ability to directly control its 6 DoFs is shown in Sec. §IV to perform better in path tracking than do the standard multicopters.

In this paper, the canted-rotor configuration of fixed-tilt hexacopters [6] is defined and illustrated in Sec. §III.A, and each rotor axis defines the rotor's position and orientation in the body frame via a position vector and a rotation matrix, respectively. Theses rotor-to-body position vectors and rotation matrices are later involved in the vehicle's equations of motion in Sec. §III.D.

This paper presents the mathematical model of the canted-rotor hexacopters. The control designs are also formulated to realize path tracking control and unique tilt-hovering control maneuvers for canted-rotor hexacopter UAVs using the linear quadratic regulator (LQR) design technique. In Sec. §III, the canted rotor-axes and forces and control input are defined, and the UAV dynamics are derived using the Newton-Euler formalism [12]. In Sec. §IV, the hexacopter dynamics is linearized, and the tracking errors of translational and rotational DoFs are defined in order to design linear controllers using LQR method. In Sec. §V, the simulation results of both path tracking and tilt-hovering controllers are presented and evaluated. And In Sec. §VI, the conclusions are reached that the simulated control designs live up to the authors' expection, and future work for this project is discussed.

# III. System Modeling

In order to describe the dynamics of canted-rotor hexacopters, we define the Earth-fixed inertial frame  $\mathcal{F}_E$ :  $\{O_E - X_E Y_E Z_E\}$ , the body frame  $\mathcal{F}_B$ :  $\{O_B - X_B Y_B Z_B\}$ , and the local frame of the *i*-th rotor  $\mathcal{F}_{m_i}$ :  $\{O_{m_i} - X_{m_i} Y_{m_i} Z_{m_i}\}$  with  $i=1\ldots 6$  as Cartesian coordinate systems. The Earth-fixed inertial frame  $\mathcal{F}_E$  denotes the inertial frame of reference fixed on the earth and its origin and three axes align with those of the body frame respectively before the vehicle takes off. The body frame  $\mathcal{F}_B$  is fixed on the vehicle body and its origin coincides with the center of mass(CoM) of the vehicle. The three axes of body frame conform to the NED convention [13], with X-axis pointing out the nose of the vehicle, Z-axis pointing out the bottom of the vehicle, and Y-axis pointing to the right. The origin of each rotor's local frame is located at the center of this motor-propeller group, while its three axes are determined by its tilting angles

as defined in Sec.§III.A. Once the coordinate systems are defined, the equations of motions of the hexacopter UAV are derived in Sec.§III.D.

#### A. Canted Rotor-Axes Definitions

The definition of the *i*-th rotor-axis orientation vector with  $i=1\dots 6$  is schematically demonstrated in Fig. 1. The body frame  $\mathcal{F}_B$  is centered at point  $O_B$ , which is the center of mass of the vehicle. And the  $X_B$ -axis of  $\mathcal{F}_B$  points out the hexacopter's nose, the  $Z_B$ -axis points out the bottom, and  $Y_B$  points out the right side. Point  $O_{m_i}$  is the center of mass of the motor-propeller group, which also defines the origin of the *i*-th local frame  $\mathcal{F}_{m_i}$ . Since  $O_{m_i}$  is defined to be on the XY-plane of  $\mathcal{F}_B$ , the length of the *i*-the rotor arm  $L_{arm}$  and the *i*-th rotor arm's yaw angle  $\psi_i$  are sufficient to locate the position of  $O_{m_i}$  in  $\mathcal{F}_B$  as in Eq. 2. And the *i*-th rotor-axis vector before tilting  $V_i$  is defined by a unit vector of the coordinates  $[0,0,-1]^T$  in the body frame. At first, the thrust vector is rotated by an angle  $\phi_i$  around the first imaginary pivot axis which passes through point  $O_{m_i}$  and is parallel to X-axis of the body frame, which gives a vector  $V_i' = [0, \sin\phi_i, -\cos\phi_i]^T$ . Secondly, the rotor-axis vector is rotated by an angle  $\theta_1$  around the second imaginary pivot axis passing through point  $O_{m_i}$  and parallel to Y-axis of the body frame. The final orientation vector of *i*-th motor-propeller group is  $V_i'' = [-\cos\phi_i \sin\theta_i, -\sin\phi_i, -\cos\phi_i \cos\theta_i]^T$ .

The rotated rotor-axis orientation vector also helps define the three axes of the *i*-th local frame, with  $V_i''$  pointing out the direction  $[0,0,-1]^T$  in the local frame, thus defining the  $Z_{m_i}$ -axis. The  $X_{m_i}$ -axis of *i*-th local frame is perpendicular to both  $V_i''$  and the rotation pivot of  $\theta_i$ . Since the  $\theta_i$  pivot is parallel to  $Y_B$ -axis of the body frame, we can calculate the cross product between  $V_i''$  and Y-axis unit vector to find the unit vector indicating the X-axis of *i*-th local frame to be  $[\cos\theta_i,0,-\sin\theta_i]^T$  in the body frame. And the Y-axis unit vector in *i*-th local frame is calculated by taking the cross product between  $Z_{m_i}$ - and  $Y_{m_i}$ -axis unit vector, rendered as  $[-\sin\phi_i\sin\theta_i,\cos\phi_i,-\sin\phi_i\cos\theta_i]^T$  in the body frame.

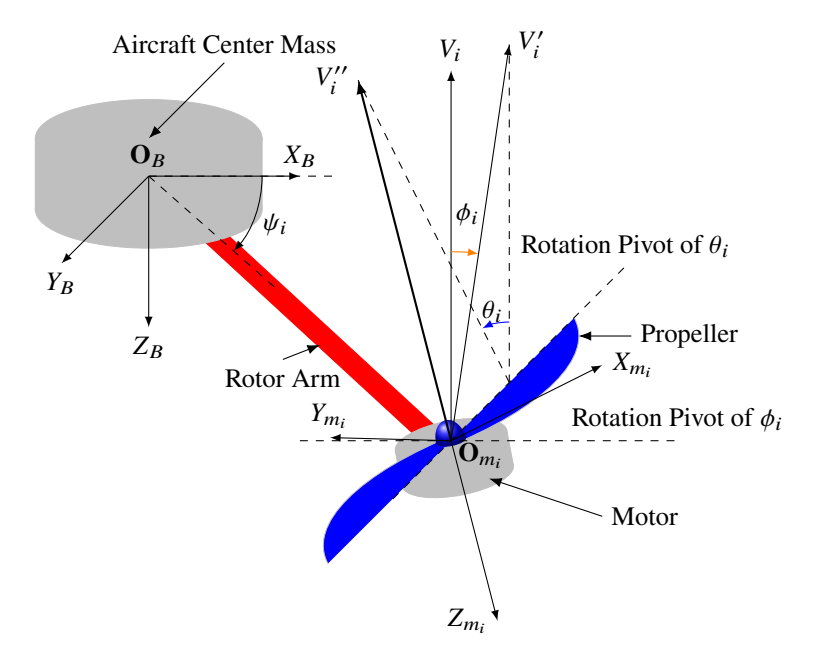


Figure 1 The illustration of canted rotor-axes.

After defining the rotor-axis orientation vectors, each rotor-axis can be characterized by a pair of rotation angles  $(\phi_i, \theta_i)$ . An illustration of a rotor-axis layout with defined orientation vectors  $V_i$  in the body frame is presented in Fig. 2. The rotor-axis notation numbers 1 through 6 are defined along the counter-clockwise sequence when looking from above (negative *Z*-direction in the body frame).

In the equations of motion that are introduced in Sec.§III.D, the characterizations of the canted-rotor axes are needed in matrix form to describe the directions of force and moment generated by each motor-propeller group. Thus, the rotation matrix  $\mathbf{R}_{Bm_i} \in \mathbb{R}^{3\times 3}$  with  $i = 1 \dots 6$  is formulated such that the force and moment in the local frame of i-th

rotor can be transformed into the body frame:

$$\mathbf{R}_{Bm_i} = \begin{bmatrix} \cos\theta_i & \sin\phi_i & \cos\phi_i \sin\theta_i \\ 0 & -\cos\phi_i & \sin\phi_i \\ -\sin\theta_i & \cos\theta_i & \sin\phi_i & \cos\phi_i \cos\theta_i \end{bmatrix}$$
(1)

Due to the fact that each rotor-axis has 2 rotational degrees of freedom based on the definition above, all 6 rotor axes can introduce a total of 12 degrees of freedom which increases the complexity of the hexacopter layout definition. For simplification, the symmetry about the *X-Z* plane of the body frame is adopted such that all the rotor-axis orientations can be described by two 3-tuples  $\mathbf{\Phi} = (\phi_1, \phi_2, \phi_3)$  and  $\mathbf{\Theta} = (\theta_1, \theta_2, \theta_3)$  of the rotation angles around their rotation pivots:

$$\phi_1 = -\phi_6, \phi_2 = -\phi_5, \phi_3 = -\phi_4;$$
  
 $\theta_1 = \theta_6, \theta_2 = \theta_5, \theta_3 = \theta_4.$ 

In addition, we also need to locate the positions of *i*-th rotor center  $O_{m_i}$  with  $i=1\ldots 6$  in the body frame  $\mathcal{F}_B$  for dynamic modelling. The position of each  $O_{m_i}$  in  $\mathcal{F}_B$  is described by a vector  $\mathbf{p}_{Bm_i}$ . For simplicity, we set all rotor arms to be equally long and all  $O_{m_i}$  to be coplanar with the origin of the body frame  $O_B$ , thus leaving 2 degrees of freedom in  $\mathbf{p}_{Bm_i}$ . In order to determine  $\mathbf{p}_{Bm_i}$ , we need the rotor arm length  $L_{arm}$  and the *i*-th rotor arm's yaw angle  $\psi_i$  in X-Y plane of  $\mathcal{F}_B$  as illustrated in Fig. 1. For a layout of normal hexagonal rotor positions, the *i*-th rotor arm's yaw angle is  $\psi_i = \pi/6 + (i-1) \cdot \pi/3$  with respect to the body X-axis. And the *i*-th rotor's position vector  $\mathbf{p}_{Bm_i}$  in  $\mathcal{F}_B$  can be calculated via:

$$\mathbf{p}_{Bm_i} = \begin{bmatrix} \cos\psi_i & -\sin\psi_i & 0\\ \sin\psi_i & \cos\psi_i & 0\\ 0 & 0 & 1 \end{bmatrix} \cdot \begin{bmatrix} L_{arm} \\ 0\\ 0 \end{bmatrix}$$
 (2)

#### **B.** Transformation Matrices

The transformation matrix for linear positions, velocities, and accelerations components from the hexacopter's body frame to the Earth-fixed inertial frame needs to be derived based on the rotation angles about the North, East, and Down directions of the inertial frame. Given that the NED convention of the inertial frame corresponds to the real-world North, East, and Down directions, and the body frame is defined by pointing out the nose, the right side, and the bottom of the vehicle body, the body-to-inertial transformation matrix  $\mathbf{R}_{EB}$  can be represented by:

$$\mathbf{R}_{EB} = \begin{bmatrix} c\theta c\psi & s\theta s\phi c\psi - c\phi s\psi & c\phi s\theta c\psi + s\phi s\psi \\ s\psi c\theta & s\phi s\theta s\psi + c\phi c\psi & s\psi s\theta c\phi - c\psi s\phi \\ -s\theta & c\theta s\phi & c\phi c\theta \end{bmatrix}$$
(3)

where "c" and "s" represent " $\cos()$ " and " $\sin()$ " in Eq. (3), respectively, and  $\theta$ ,  $\phi$ ,  $\psi$  are the pitch, roll, and yaw body rotation angles between the body frame's North, East, Down axes and those of the frame, respectively. Similarly, the rotation angles, angular rates and accelerations measured in the body frame need to be transformed to the inertial frame by another transformation matrix:

$$\mathbf{T}_{EB} = \begin{bmatrix} 1 & \sin\phi \tan\theta & \cos\phi \tan\theta \\ 0 & \cos\phi & -\sin\phi \\ 0 & \frac{\sin\phi}{\cos\theta} & \frac{\cos\phi}{\cos\theta} \end{bmatrix}$$
(4)

#### C. Forces and Control Input

Next, the thrust forces generated by i-th motor-propeller group, where  $i = 1 \dots 6$ , is derived. For each rotor, the propulsive force produced by the spinning of its propeller is approximated by a quadratic equation of the angular speed of the propeller:

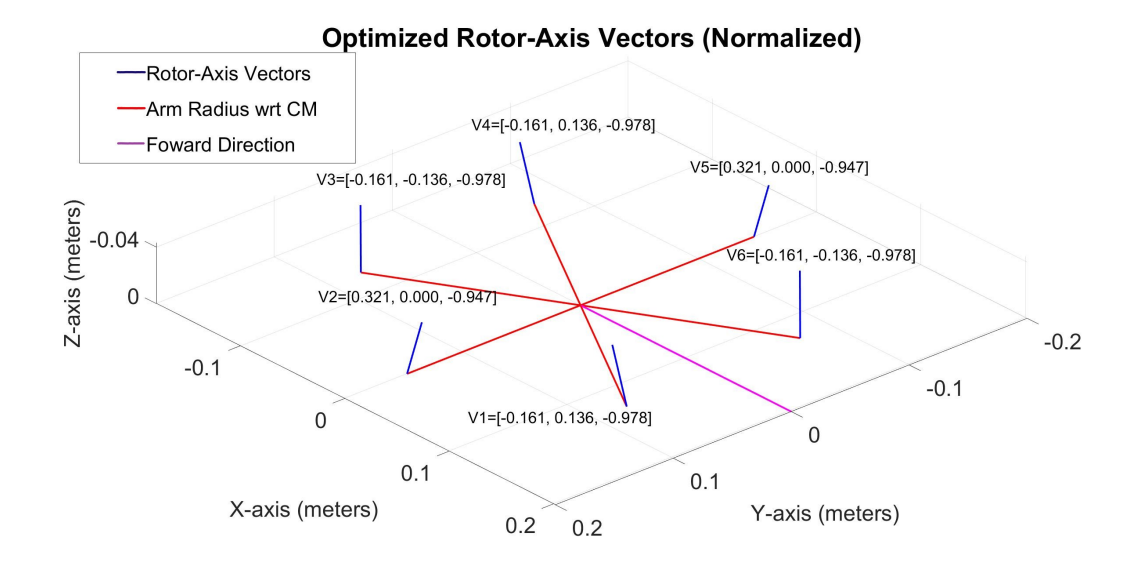


Figure 2 An example of canted rotor-axes layout in the body frame

$$T_i = k_f \cdot \omega_i^2 \tag{5}$$

where  $k_f$  is a coefficient related to the area of the rotor disk and air density, which is regarded as a constant in our scenario.  $\omega_i$  is the angular speed of the *i*-th propeller. In a thrust testing experiment of the selected motor-propeller group in this paper, the measured thrusts of a rotor fit well with a second-order equation the angular speed where  $k_f$  estimated to be  $9.23 \times 10^{-7} \ N \cdot s^2/rad^2$ , thus verifying Eq. (5).

Each rotor also generates a moment due to the propeller's drag, which acts in the opposite direction of the propeller angular speed. This moment of i-th motor-propeller group can be approximated by:

$$M_i = -k_m \cdot \omega_i |\omega_i| \tag{6}$$

where  $k_m$  is the drag moment coefficient, which calculated via an equation based on the blade element theory incorporating air density, angle of resultant flow, propeller chord length, total blade area, and propeller drag coefficient[14]. In case of the selected motor-propeller assembly in this paper,  $k_m$  is calculated to be  $2.73 \times 10^{-8} \ Nm \cdot s^2/rad^2$ . In order to determine the signs of  $\omega_i$  with  $i = 1 \dots 6$ , we use a typical hexacopter rotation pattern, with 1 and -1 indicating the counter-clockwise and clockwise rotation direction with respect to the Z-axis of the i-th local frame  $\mathcal{F}_{m_i}$ :

$$\mathbf{sgn}(\omega_i) = (-1)^i, \ i = 1 \dots 6 \tag{7}$$

In the *i*-th local frame  $\mathcal{F}_{m_i}$ , both vectors of  $\mathbf{F}_{m_i} \in \mathbb{R}^3$  and  $\mathbf{M}_{m_i} \in \mathbb{R}^3$  are along Z-direction, such that:

$$\mathbf{F}_{m_i} = \begin{bmatrix} 0 \\ 0 \\ -k_f \omega_i^2 \end{bmatrix}, \mathbf{M}_{m_i} = \begin{bmatrix} 0 \\ 0 \\ (-1)^{i+1} k_m \omega_i^2 \end{bmatrix}$$
(8)

We notice that both  $\mathbf{F}_{m_i}$  and  $\mathbf{M}_{m_i}$  are proportional to the square of the spinning speed *i*-th propeller  $\omega_i$ , thus the intermediate force vector  $\Omega \in \mathbb{R}^6$  of the system is defined as:

$$\Omega = [\omega_1^2 \ \omega_2^2 \ \omega_3^2 \ \omega_4^2 \ \omega_5^2 \ \omega_6^2]^T \tag{9}$$

The brushless DC motor dynamics is set to be controlled by a electronic speed controller (ESC) via pulse width modulation (PWM) duty cycles. The ESC receives PWM signals from  $1000 \ \mu s$  to  $2000 \ \mu s$  in each  $20 \ ms$  cycle to

control the voltage input to the motor, thus controlling the angular speed. In another thrust testing experiment conducted by authors, the selected rotor group is investigated to collect data point of PWM signals and  $\omega^2$  at various steady states. We found for the selected motor-propeller assembly,  $\omega^2$  fits well in a second-order polynomial of the PWM signals as:

$$\omega^2 = a \cdot PWM^2 + b \cdot PWM + c \tag{10}$$

where  $\omega$  is in the unit rad/s and PWM is in  $\mu s$ , a, b, and c are polynomial coefficients, while in the 2 case studies in this paper, the motor and propeller are selected to be Lumenier RX2206-11 2350kv brushless motor and Lumenier 5x4.5" 2-blade propeller, respectively, and their coefficients are found to be 3.5191,  $-4.2585 \times 10^3$ , and  $8.0159 \times 10^5$ , respectively. However, the brushless motors are identified to be first-order filter in its response to PWM signals[15], such that we assume this motor-propeller group is also a first-order dynamic system when responding to the PWM inputs which adjusts the input voltage. The corresponding first-order transfer function is modelled as:

$$G(s) = \frac{\omega(s)}{PWM(s)} = \frac{K}{\tau_0 s + 1} \tag{11}$$

Setting K = 1 and estimating  $\tau_0 = 0.2$  s from experimental data, we map the intermediate force vector  $\Omega$  to the *PWM* input of each motor by:

$$\Omega(PWM_{i},t) = \begin{bmatrix}
\omega_{1,t_{0_{1}}}^{2} + (1 - e^{-0.2(t-t_{0_{1}})}) \cdot (\omega_{1,t}^{2} - \omega_{1,t_{0_{1}}}^{2}) \\
\omega_{2,t_{0_{2}}}^{2} + (1 - e^{-0.2(t-t_{0_{2}})}) \cdot (\omega_{2,t}^{2} - \omega_{2,t_{0_{2}}}^{2}) \\
\vdots \\
\omega_{6,t_{0_{6}}}^{2} + (1 - e^{-0.2(t-t_{0_{6}})}) \cdot (\omega_{6,t}^{2} - \omega_{6,t_{0_{6}}}^{2})
\end{bmatrix}$$
(12)

where  $t_{0i}$  is the moment of receiving the latest PWM command in *i*-th channel.

#### **D. Newton-Euler Equations of Motion**

## 1. Translational Dynamics

We express the translational dynamics of the canted-rotor hexacopter model in the inertial frame  $\mathcal{F}_E$ , using the standard Newton-Euler equation:

$$m\ddot{\xi} = m \begin{bmatrix} 0 \\ 0 \\ g \end{bmatrix} + \mathbf{R}_{EB} \sum_{i=1}^{6} \mathbf{R}_{Bm_i} \mathbf{F}_{m_i} + \mathbf{F}_{ext}$$

$$\tag{13}$$

where m is the mass of the aircraft,  $\xi \in \mathbb{R}^3$  is the hexacopter's linear position  $[x_E, y_E, Z_E]^T$  in the inertial frame  $\mathcal{F}_E$ , g is the gravitational acceleration, and  $\mathbf{F}_{ext} \in \mathbb{R}^3$  is the external disturbance forces. In our case,  $\mathbf{F}_{ext}$  consists of the in-flight drag force acting in the opposite direction of the linear velocities, and unmodelled aerodynamic and structural effects as:

$$\mathbf{F}_{ext} = \mathbf{R}_{EB} \begin{bmatrix} -C_{D_x} \cdot \dot{x}_B | \dot{x}_B | \\ -C_{D_y} \cdot \dot{y}_B | \dot{y}_B | \\ -C_{D_z} \cdot \dot{z}_B | \dot{z}_B | \end{bmatrix} + \text{unmodelled effects}$$
(14)

where  $C_{D_x}$ ,  $C_{D_y}$ ,  $C_{D_z}$  are the coefficients to calculate drag forces in the body frame  $\mathcal{F}_B$  as modelled in [16],  $\dot{x_B}$ ,  $\dot{y_B}$ ,  $\dot{z_B}$  are the velocity components in  $\mathcal{F}_B$ .

#### 2. Rotational Dynamics

Adding up the inertial term, the torques produced by rotor thrusts and drag moments, and the external disturbances on the right-hand side, we can formulate the rotational dynamics of the hexacopter in the body frame  $\mathcal{F}_B$  using the Newton-Euler equation of motion:

$$\mathbf{I}_{\mathbf{B}}\dot{\eta}_{B} = -\eta_{B} \times \mathbf{I}_{B}\eta_{B} + \sum_{i=1}^{6} \mathbf{p}_{Bm_{i}} \times \mathbf{R}_{Bm_{i}}\mathbf{F}_{m_{i}} + \sum_{i=1}^{6} \mathbf{R}_{Bm_{i}}\mathbf{M}_{m_{i}} + \tau_{ext}$$

$$\tag{15}$$

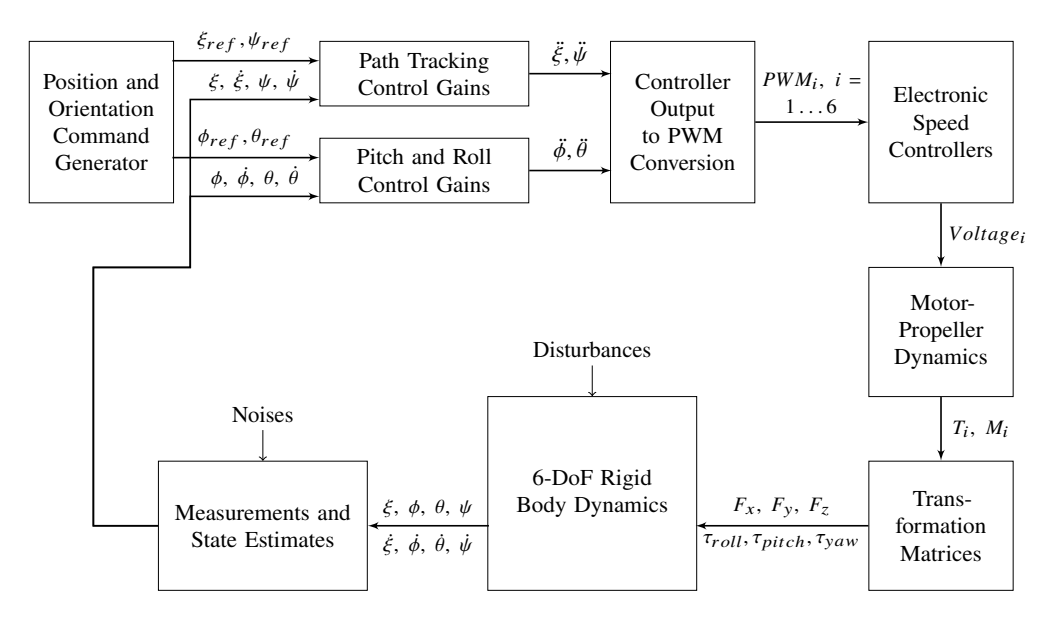


Figure 3 Hexacopter control scheme architecture.

where  $\mathbf{I}_B \in \mathbb{R}^{3\times 3}$  is the hexacopter inertia matrix in  $\mathcal{F}_B$ ,  $\eta_B \in \mathbb{R}^3$  is the the angular rates  $[p,q,r]^T$  in  $\mathcal{F}_B$ , and  $\tau_{ext} \in \mathbb{R}^3$  accounts for the external disturbances torques. The rotational rates and accelerations in  $\mathcal{F}_B$  can be transformed to those in  $\mathcal{F}_E$  by left multiplying  $\mathbf{T}_{EB}$  in Eq. (4):

$$\dot{\eta}_E = \mathbf{T}_{EB} \cdot \dot{\eta}_B, \, \eta_E = \mathbf{T}_{EB} \cdot \eta_B \tag{16}$$

This transformation equation is applied primarily in the tilt-hovering control as discussed in Sec.§IV.E, but can be neglected when applying path tracking control since the roll and pitch angles remain close to zero making  $T_{EB}$  nearly identity matrix.

#### IV. Control Design

In this section, the control strategies of the both path tracking controller and tilt-hovering controller are described. The overall block diagram of the feedback control system is shown in Fig. 3. The purpose of control designs here is to decouple the translational and rotational dynamics of the hexacopter, and to ensure that the hexacopter can follow a desired path of its translational states without performing pitch and roll rotations in the "path tracking" mode, as well as tracking a controlled purely rotational trajectory of vehicles' states while keeping its center-of-mass stationary in the inertial frame when switched to the "tilt-hovering" mode.

#### A. Model Linearization

In order to rapidly compute the desired control input, the system model is linearized between the output states  $\ddot{\xi}$ ,  $\dot{\eta}_B$  and intermediate force vector  $\Omega$  which further maps to the *PWM* commands as system input. First, since both  $\mathbf{F}_{m_i}$  and  $\mathbf{M}_{m_i}$  are linearly dependent on  $\omega_i$ , we can formulate the linear terms in Eq. (13) and (15) as:

$$\mathbf{B}_{F}\Omega(PWM_{i},t) = \frac{1}{m}\mathbf{R}_{EB}\sum_{i=1}^{6}\mathbf{R}_{Bm_{i}}\mathbf{F}_{m_{i}}$$

$$\mathbf{B}_{\tau}\Omega(PWM_{i},t) = \mathbf{I}_{B}^{-1}(\sum_{i=1}^{6}\mathbf{p}_{Bm_{i}}\times\mathbf{R}_{Bm_{i}}\mathbf{F}_{m_{i}} + \sum_{i=1}^{6}\mathbf{R}_{Bm_{i}}\mathbf{M}_{m_{i}})$$
(17)

where  $\mathbf{B}_F \in \mathbb{R}^{3\times 6}$  and  $\mathbf{B}_{\tau} \in \mathbb{R}^{3\times 6}$  are linear mapping matrices for  $\Omega$ . In this case, we ignore the non-linear disturbances terms in (13) and (15), combine overall linear and rotational accelerations to vector  $\mathbf{a} \in \mathbb{R}^6$ , and view gravitational and

inertial-related angular acceleration terms as generalized internal forces and formulate them as vector  $\mathbf{q} \in \mathbb{R}^6$ :

$$\mathbf{a} = \begin{bmatrix} \ddot{\mathcal{E}}_{[3\times1]} \\ \dot{\eta}_{B[3\times1]} \end{bmatrix}, \mathbf{q} = \begin{bmatrix} 0 \\ 0 \\ g \\ -\mathbf{I}_{B}^{-1}(\eta_{B} \times \mathbf{I}_{B}\eta_{B})_{[3\times1]} \end{bmatrix}$$
(18)

thus the dynamic equations in (13) and (15) can be linearized as:

$$\mathbf{a} - \mathbf{q} = \mathbf{B}\Omega \tag{19}$$

where  $\mathbf{B} = [\mathbf{B}_F \ \mathbf{B}_\tau]^T \in \mathbb{R}^{6\times 6}$ . When  $\mathbf{B}$  is of full rank,  $\Omega$  can be calculate by left multiplying  $\mathbf{B}^{-1}$  on both sides. Even if  $\mathbf{B}$  is rank-deficient,  $\Omega$  could still be solved using Moore-Penrose pseudo-inverse. Once the desired  $\Omega$  is found, the desired PWM command for each motor can be mapped using (10), and the saturation limits of each motor shall be met as well.

## **B.** Tracking Error Dynamics

The proportional-integral-derivative (PID) feedback control strategy is implemented to track the reference signals and stabilize the hexacopter states. Since the lateral body force components in  $\sum_{i=1}^{6} \mathbf{R}_{Bm_i} \mathbf{F}_{m_i}$  can be decoupled from the pitch and roll angles, we can discard the traditional multicopter control architecture in which the attitude control serves as lower-level controller. Instead, the attitude controller and position controller can track uncorrelated reference signals. In this case, tracking errors in all 6 DoFs are needed in order to design the state feedback controllers. The position, linear velocity and acceleration errors of the hexacopter in the inertial frame  $\mathcal{F}_E$  are:

$$e_{x} = x - x_{ref}, \dot{e}_{x} = \dot{x} - \dot{x}_{ref}, \ddot{e}_{x} = \ddot{x} - \ddot{x}_{ref}$$

$$e_{y} = y - y_{ref}, \dot{e}_{y} = \dot{y} - \dot{y}_{ref}, \ddot{e}_{y} = \ddot{y} - \ddot{y}_{ref}$$

$$e_{z} = z - z_{ref}, \dot{e}_{z} = \dot{z} - \dot{z}_{ref}, \ddot{e}_{z} = \ddot{z} - \ddot{z}_{ref}$$
(20)

thus we can formulate a position error state vector  $\mathbf{e}_{\xi}$  and introduce the error input vector  $\mathbf{u}_{\xi}$  in terms of the second-order error as:

$$\mathbf{e}_{\xi} = \begin{bmatrix} e_x & \dot{e}_x & \int_{t_0}^t e_x dt & e_y & \dot{e}_y & \int_{t_0}^t e_y dt & e_z & \dot{e}_z & \int_{t_0}^t e_z dt \end{bmatrix}^T, \quad \mathbf{u}_{\xi} = \begin{bmatrix} \ddot{e}_x & \ddot{e}_y & \ddot{e}_z \end{bmatrix}^T, \tag{21}$$

such that the dynamics of position tracking error in  $\mathcal{F}_E$  is formulated in the similar pattern of state-space equation as in [7]:

$$\dot{\mathbf{e}}_{\xi} = A_{\xi} \mathbf{e}_{\xi} + B_{\xi} \mathbf{u}_{\xi}, \tag{22}$$

where

In this scenario, the controllability matrix  $\mathcal{C}(A_{\xi}, B_{\xi})$  is of full rank, such that  $(A_{\xi}, B_{\xi})$  is controllable. Similarly, an orientation error state vector can be formulated as  $\mathbf{e}_{R} = [e_{\phi}, \dot{e}_{\phi}, \int_{t_{0}}^{t} e_{\phi} dt, e_{\theta}, \dot{e}_{\theta}, \int_{t_{0}}^{t} e_{\theta} dt, e_{\psi}, \dot{e}_{\psi}, \int_{t_{0}}^{t} e_{\psi} dt]^{T}$ , the rotational error vector can be given as  $\mathbf{u}_{R} = [\ddot{e}_{\phi}, \ddot{e}_{\theta}, \ddot{e}_{\psi}]^{T}$ , and the dynamics of orientation tracking error is rendered as:

$$\dot{\mathbf{e}}_R = A_R \mathbf{e}_R + B_R \mathbf{u}_R,\tag{24}$$

with  $A_R = A_{\xi}$ ,  $B_R = B_{\xi}$ .

#### C. Linear Quadratic Control Design

In order to design a state feedback controller  $\mathbf{u} = -K\mathbf{e}$  where  $K \in \mathbb{R}^{3\times 9}$  to stabilize the error dynamics and converge fast, we implement the optimal control design approach of Linear Quadratic Regulator [17]. In order to minimize a cost function

$$J = \int_0^\infty \mathbf{e}^T Q \mathbf{e} + \mathbf{u}^T R \mathbf{u} dt, \tag{25}$$

with Q and R selected based on control requirements, the gain matrix K is determined by  $K = R^{-1}B^TP$ , where P matrix is the solution to the continuous-time algebraic Ricatti equation

$$A^{T}P + PA - PBR^{-1}B^{T}P + Q = 0. (26)$$

Applying LQR to our PID control scheme, the obtained gain matrix *K* includes the gain for each of the proportional, integral, and derivative tracking errors in each of the 3 DoFs. Take the translational 3 DoFs as an example, the gain matrix can be written as:

$$K_{\xi} = \begin{bmatrix} k_{p,x} & k_{d,x} & k_{i,x} & 0 & 0 & 0 & 0 & 0 & 0 \\ 0 & 0 & 0 & k_{p,y} & k_{d,y} & k_{i,y} & 0 & 0 & 0 \\ 0 & 0 & 0 & 0 & 0 & k_{p,z} & k_{d,z} & k_{i,z} \end{bmatrix}$$
(27)

such that the second-order state vector to be controlled is given as:

$$\ddot{\xi} = \begin{bmatrix} \ddot{x}_{ref} - k_{p,x} e_x - k_{d,x} \dot{e}_x - k_{i,x} \int_{t_0}^t e_x dt \\ \ddot{y}_{ref} - k_{p,y} e_y - k_{d,y} \dot{e}_y - k_{i,y} \int_{t_0}^t e_y dt \\ \ddot{z}_{ref} - k_{p,z} e_z - k_{d,z} \dot{e}_z - k_{i,z} \int_{t_0}^t e_z dt \end{bmatrix}$$
(28)

Similarly,  $\dot{\eta}_B$  can also be controlled using gains obtained from LQR design approach as well, and these control signals can be used to solve for  $\Omega$  vector as in Eq. (19), and  $\Omega$  can be mapped to discretized PWM commands to control 6 rotors.

#### **D. Path Tracking Controller**

In order to track the 3-dimensional position trajectories, the controllers need to possess enough authority and control bandwith to generate flat output states tracking closely reference signals in X, Y, Z and yaw directions in  $\mathcal{F}_E$  [11], while the pitch and yaw controller only serve to track zero setpoints and resist disturbance torque. For the path tracking case study in this paper, whose  $\Phi$  and  $\Theta$ -tuple are (0.1364, 0, -0.1364) and (0.1627, -0.3268, -0.1627), respectively, and  $L_{arm} = 0.207 \ m$ , the  $Q_{\mathcal{E}}$  and  $R_{\mathcal{E}}$  matrices are selected to be

$$Q_{\xi} = diag([200, 2000, 10, 200, 2000, 10, 4000, 200, 5]^T), R_{\xi} = 2 \cdot I_3,$$
 (29)

which renders the gain matrix  $K_{\xi}$  for translational 3 degrees of freedom to be

$$K_{\xi} = \begin{bmatrix} 15.6081 & 32.1126 & 2.2361 & 0 & 0 & 0 & 0 & 0 & 0 \\ 0 & 0 & 0 & 15.6081 & 32.1126 & 2.2361 & 0 & 0 & 0 \\ 0 & 0 & 0 & 0 & 0 & 0 & 45.2066 & 13.7990 & 1.5811 \end{bmatrix}. \tag{30}$$

While the  $Q_R$  and  $R_R$  matrices for the orientation control are

$$Q_R = diag([100, 2000, 10, 100, 2000, 10, 1000, 2 \times 10^5, 100]^T), R_R = 2 \cdot I_3,$$
 (31)

which renders the gain matrix  $K_R$  for rotational 3 degrees of freedom to be

$$K_R = \begin{bmatrix} 13.9059 & 32.0595 & 2.2361 & 0 & 0 & 0 & 0 & 0 & 0 \\ 0 & 0 & 0 & 13.9059 & 32.0595 & 2.2361 & 0 & 0 & 0 \\ 0 & 0 & 0 & 0 & 0 & 0 & 30.7992 & 401.2302 & 7.0711 \end{bmatrix}$$
(32)

#### E. Tilt-Hover Controller

The concept of tilt-hover controller is based on the expectation to hover the hexacopter at a certain altitude and rotate it to a pose with certain pitch or roll angle, while the its center of mass can remain stationary because of the special configuration of the canted-rotor hexacopter. This objective requires the hexacopter to have special configuration of rotor-axes canted to adequate amount according to the desired rotation angle, and its controller to have enough control authority and bandwith in pitch and roll rotational direction. For the tilt-hover control case study in this paper, whose  $\Phi$  and  $\Theta$ -tuple are (0.4115, 0, -0.4115) and (0.3338, -0.6971, -0.3338), respectively, and  $L_{arm} = 0.207 m$ , the  $Q_{\xi}$  and  $R_{\xi}$  matrices are selected to be

$$Q_{\xi} = diag([50, 200, 1, 50, 200, 1, 4000, 200, 5]^T), R_{\xi} = 2 \cdot I_3,$$
 (33)

which renders the translational gain matrix  $K_{\mathcal{E}}$ :

$$K_{\xi} = \begin{bmatrix} 6.3253 & 10.6137 & 0.7071 & 0 & 0 & 0 & 0 & 0 & 0 \\ 0 & 0 & 0 & 6.3253 & 10.6137 & 0.7071 & 0 & 0 & 0 \\ 0 & 0 & 0 & 0 & 0 & 0 & 45.2066 & 13.7990 & 1.5811 \end{bmatrix}$$
(34)

While the  $Q_R$  and  $R_R$  matrices for the orientation control in tilt-hovering mode are selected as

$$Q_R = diag([1 \times 10^5, 2 \times 10^6, 100, 1 \times 10^5, 2 \times 10^6, 100, 1000, 2 \times 10^4, 10]^T), R_R = 2 \cdot I_3, \tag{35}$$

which produce the rotational gain matrix  $K_R$  for tilt-hovering:

$$K_R = \begin{bmatrix} 253.2700 & 1000.253 & 7.0711 & 0 & 0 & 0 & 0 & 0 & 0 \\ 0 & 0 & 0 & 253.2700 & 1000.253 & 7.0711 & 0 & 0 & 0 \\ 0 & 0 & 0 & 0 & 0 & 0 & 30.7992 & 100.3075 & 2.2361 \end{bmatrix}$$
(36)

#### **V. Simulation Results**

#### A. Path Tracking Simulations

# 

Figure 4 Comparison of square path tracking.

The validation of the path tracking controller designed in Sec. §IV.D is conducted with a simulation tracking a  $50m \times 50m$  square path and another simulation tracking a circular path of 1.5m radius at 1.5m altitude above ground  $(z_E = -1.5m \text{ in NED coordinates})$ . As shown in Fig. 4, the square path consists of waypoints in a sequence of  $[0, 0, -1.5]^T$ ,  $[50, 0, -1.5]^T$ ,  $[50, 50, -1.5]^T$ ,  $[0, 50, -1.5]^T$ ,  $[0, 0, -1.5]^T$ . And the circular path with its center located

at  $[-0.25, 0, -1.5]^T$  is shown in Fig. 5. For the path tracking case study in this paper, the canted-rotor hexacopter to be simulated with its  $\Phi$  and  $\Theta$ -tuple to be (0.1364, 0, -0.1364) and (0.1627, -0.3268, -0.1627), respectively, and  $L_{arm} = 0.207 \ m$ . The mass of the canted-rotor hexacopter is m = 0.754kg, and the moments of inertia  $I_B = diag([5.5 \times 10^{-3}, 5.8 \times 10^{-3}, 1.09 \times 10^{-2}]^T)kg \cdot m^2$ . The standard hexacopter is of the same size, mass, moments of inertia, and thrust range of the canted-rotor one.

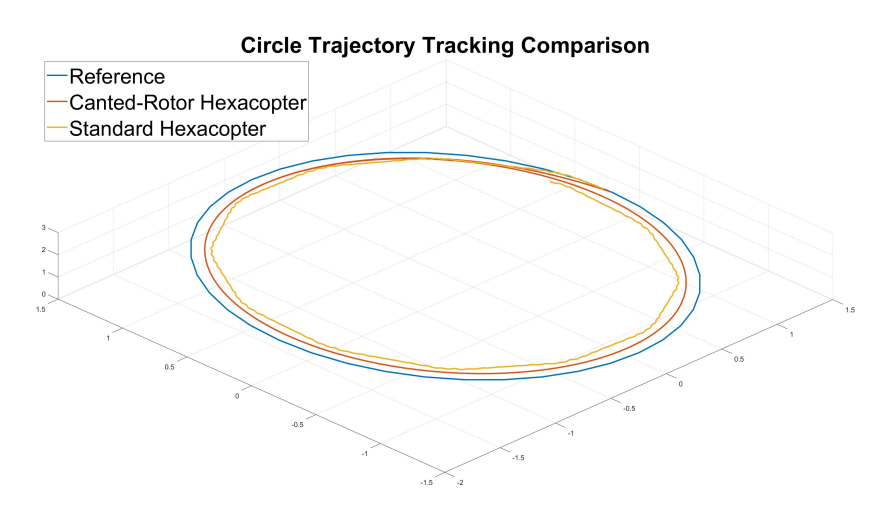


Figure 5 Circular path tracking.

In the square path simulation, the desired path is marked by 4,000 look-ahead points [18] with a look-ahead distance of 10m to avoid significant overshoots. For both canted-rotor and standard hexacopters, the maximum velocity is set to be 5m/s and the time scope of both simulations is 80 seconds. And the  $\mathbf{F}_{ext}$  is modelled according to Eq. 14 with each  $C_{D_i}$  selected as 0.1. As shown in Fig. 4, the canted-rotor hexacopter outperforms the standard one which has the identical mass, moments of inertia, and thrust range of the canted-rotor one, and also incorporates carefully tuned PID control gains. The trajectory of canted-rotor hexacopter has an average cross-track error of 0.266m with respect to the entire path, while the standard hexacopter has an average cross-track error of 2.238m.

In the circular path simulation, the desired path is marked by 100 look-ahead points with a look-ahead distance of 0.5m. For both canted-rotor and standard hexacopters, the maximum velocity is set to be 1m/s and the time scope of both simulations is 40 seconds. As shown in Fig. 5, the canted-rotor hexacopter also outperforms the standard one with smoother trajectory and lower cross-track errors. The canted-rotor hexacopter's average cross-track error is  $4.2 \times 10^{-2} m$  along the path, and the standard one has an average cross-track error of  $7.1 \times 10^{-2} m$ . The oscillations on the trajectory of the standard hexacopter might be caused by the fact that it needs to frequently alternate the pitch and roll angles to output relatively small linear accelerations along the path.

#### **B. Tilt-Hover Simulations**

In order to test the tilt-hovering controller, the case study hexacopter is set to have  $\Phi = (0.4115, 0, -0.4115)$  and  $\Theta = (0.3338, -0.6971, -0.3338)$ , m = 0.754kg,  $\mathbf{I}_B = diag([5.5 \times 10^{-3}, 5.8 \times 10^{-3}, 1.09 \times 10^{-2}]^T)kg \cdot m^2$ , and  $L_{arm} = 0.207 \ m$ . The simulation rotates the drone by a certain pitch or roll angle while hovering its center of mass stationary at  $[0, 0, -1.5]^T$  in  $\mathcal{F}_E$ . Fig. 6 shows the step response plot of  $\phi_{ref} = -0.3rad$  with respect to  $\mathcal{F}_E$ , and Fig. 7 illustrates the simulation results of  $\theta_{ref} = 0.3rad$ , both are shown to reach steady state within 5 seconds. Although the hexacopter successfully hovers at the origin of  $\mathcal{F}_E$  with tilted orientations, the oscillations appear to be considerable. In Fig.7, the hexacopter first overshoots beyond -0.2rad then oscillates till stabilizing at 0.3rad. This might be caused by relatively large proportional gains compared to derivative gains in the pitch direction.

# VI. Conclusions

This paper demonstrates the mathematical model of canted-rotor hexacopter in order to enhance the control maneuverability of conventional multi-rotor systems. The system dynamics is then linearized and the tracking error

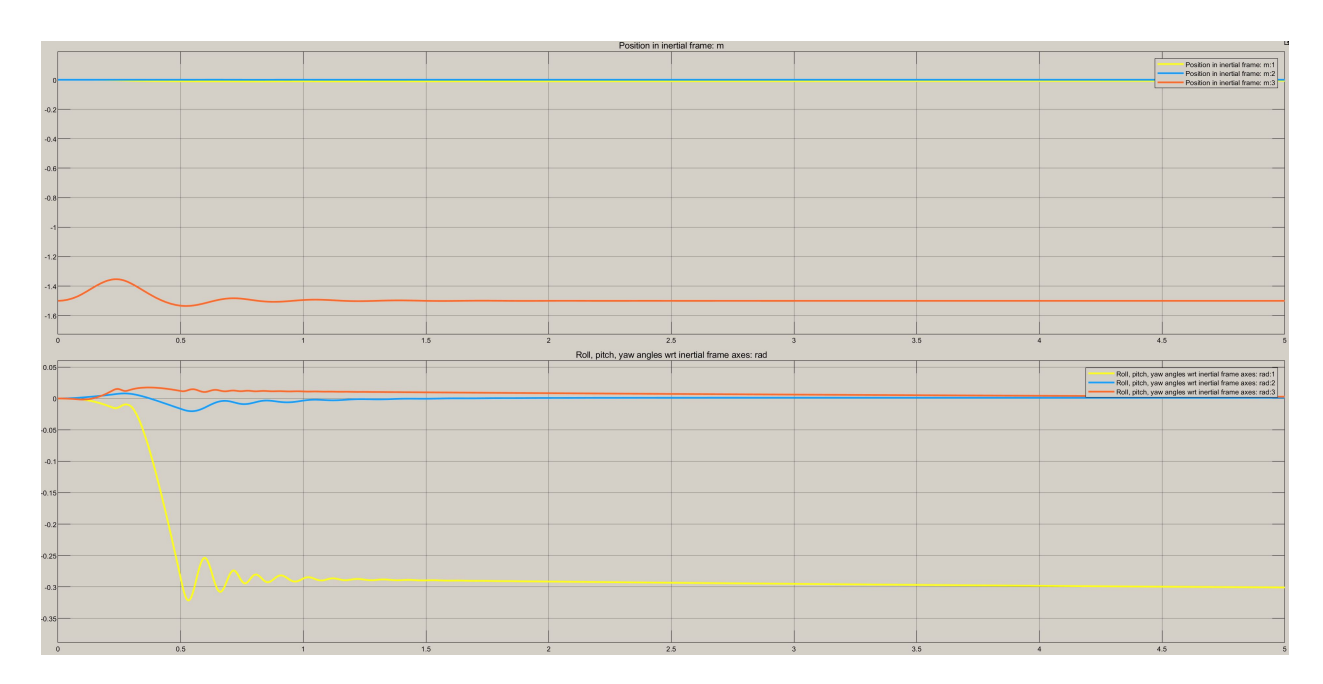


**Figure 6** Tilt-hover simulation with  $\phi_{ref} = -0.3rad$ 

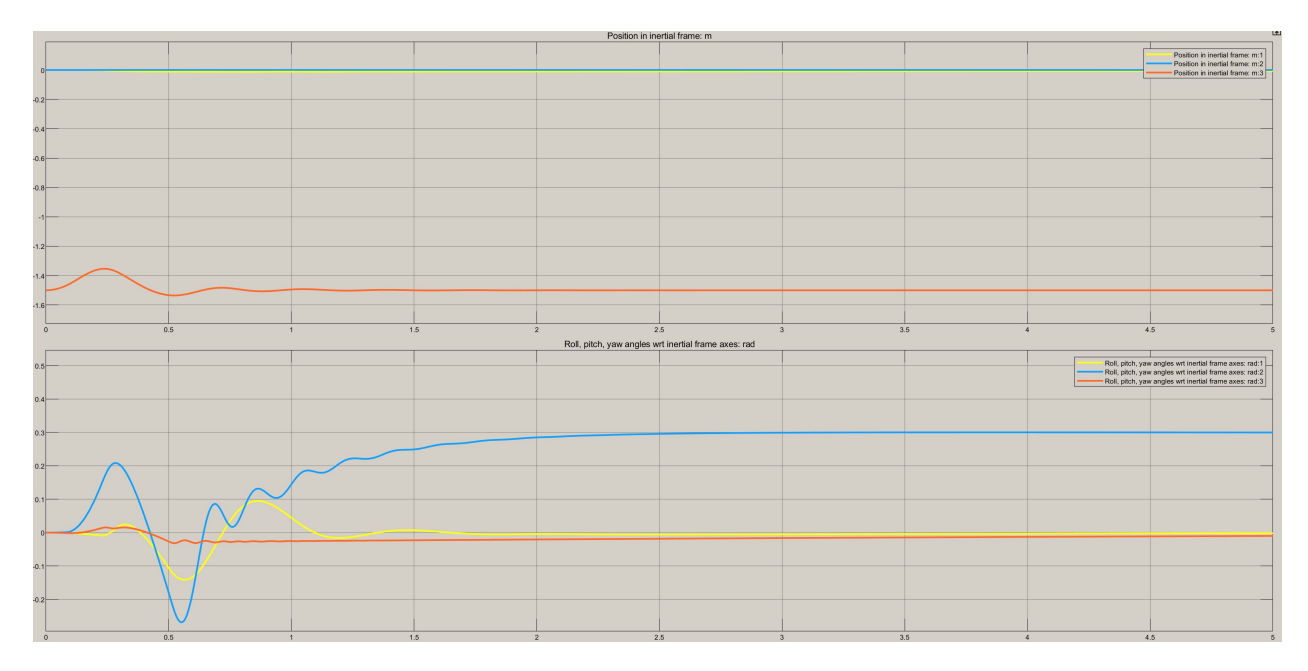


**Figure 7** Tilt-hover simulation with  $\theta_{ref} = 0.3 rad$ 

dynamics is formulated to implement the linear quadratic control design technique, based on which the path tracking and tilt-hover controllers are designed and fine-tuned. The path tracking controller decouples the lateral movements from the pitch and roll rotations of the vehicle, and the tilt-hover controller stabilizes the position of the center of mass of the vehicle as well as its heading while it is rotated by a certain pitch or roll angle, decoupling pitch and roll from lateral translations as well. Numerical simulations are then performed to corroborate the mathematical model and control designs. The path tracking controller of the canted-rotor hexacopter performs better than do the linear controller of standard hexacopter as presented in Sec. §V.A. And the tilt-hover controller lives up to the expected performance as shown in Sec. §V.B.

Despite the satisfactory simulation results, the proposed model and controllers will need to be implemented on

real-world hexacopter UAV systems with canted-rotors to be further validated in the future work. The sim-to-real gap between simulation and real-world implementation remains challenging to be resolved. The future work will also involve the path tracking and tilt-hovering experiments using data from onboard sensor and motion capture system, as well as a series of maneuvers to explore the functionality of canted-rotor hexacopters.

#### References

- 1. Wypych, T., Strawson, J., Petrovic, V., Angelo, R., Hoff, A., Howland, M., Seracini, M., Levy, T. & Kuester, F. Airborne imaging for cultural heritage in 2014 IEEE Aerospace Conference (2014), 1–9.
- 2. Ruggiero, F., Lippiello, V. & Ollero, A. Aerial manipulation: A literature review. *IEEE Robotics and Automation Letters* 3, 1957–1964 (2018).
- 3. Giribet, J. I., Sanchez-Pena, R. S. & Ghersin, A. S. Analysis and Design of a Tilted Rotor Hexacopter for Fault Tolerance. *IEEE Transactions on Aerospace and Electronic Systems* **52**, 1555–1567. ISSN: 2371-9877 (Aug. 2016).
- 4. Nemati, A. & Kumar, M. Modeling and control of a single axis tilting quadcopter in 2014 American Control Conference (2014), 3077–3082.
- 5. Bin Junaid, A., Diaz De Cerio Sanchez, A., Betancor Bosch, J., Vitzilaios, N. & Zweiri, Y. Design and implementation of a dual-axis tilting quadcopter. *Robotics* 7, 65 (2018).
- 6. Rashad, R., Goerres, J., Aarts, R., Engelen, J. B. C. & Stramigioli, S. Fully Actuated Multirotor UAVs: A Literature Review. *IEEE Robotics Automation Magazine* 27, 97–107 (2020).
- 7. Hernandez-Martinez, E. G., Fernandez-Anaya, G., Ferreira, E., Flores-Godoy, J. J. & Lopez-Gonzalez, A. Trajectory tracking of a quadcopter UAV with optimal translational control. *IFAC-PapersOnLine* **48**, 226–231 (2015).
- 8. Kamel, M., Verling, S., Elkhatib, O., Sprecher, C., Wulkop, P., Taylor, Z., Siegwart, R. & Gilitschenski, I. The Voliro Omniorientational Hexacopter: An Agile and Maneuverable Tiltable-Rotor Aerial Vehicle. *IEEE Robotics Automation Magazine* 25, 34–44. ISSN: 1558-223X (Dec. 2018).
- 9. Brescianini, D. & D'Andrea, R. Design, modeling and control of an omni-directional aerial vehicle in 2016 IEEE international conference on robotics and automation (ICRA) (2016), 3261–3266.
- Rajappa, S., Ryll, M., Bülthoff, H. H. & Franchi, A. Modeling, control and design optimization for a fully-actuated hexarotor aerial vehicle with tilted propellers in 2015 IEEE international conference on robotics and automation (ICRA) (2015), 4006–4013.
- 11. Mellinger, D. & Kumar, V. Minimum snap trajectory generation and control for quadrotors in 2011 IEEE International Conference on Robotics and Automation (2011), 2520–2525.
- 12. Ardema, M. D. Newton-Euler Dynamics (Springer Science & Business Media, 2006).
- 13. Cai, G., Chen, B. M. & Lee, T. H. Coordinate Systems and Transformations in Unmanned Rotorcraft Systems 23–34 (Springer London, London, 2011). ISBN: 978-0-85729-635-1.
- 14. Gill, R. & D'Andrea, R. Propeller thrust and drag in forward flight in 2017 IEEE Conference on Control Technology and Applications (CCTA) (2017), 73–79.
- 15. Hongwei Fang, Changliang Xia, Zhengwei Chen & Xile Wei. Position servo control of brushless DC motor based on the second discrete filter in 2007 IEEE International Conference on Robotics and Biomimetics (ROBIO) (2007), 1838–1842.
- 16. Stepanyan, V. & Krishnakumar, K. S. Estimation, navigation and control of multi-rotor drones in an urban wind field in AIAA information systems-AIAA infotech@ aerospace 0670 (2017).
- 17. Bemporad, A., Morari, M., Dua, V. & Pistikopoulos, E. N. The explicit linear quadratic regulator for constrained systems. *Automatica* **38**, 3–20 (2002).
- 18. Osborne, J. & Rysdyk, R. Waypoint guidance for small UAVs in wind in Infotech@ Aerospace 6951 (2005).